Biointerface Research in Applied Chemistry
Open-Access Journal (ISSN: 2069-5837)

Article
Volume 16, Issue 3, 2026, 97
https://doi.org/10.33263/BRIAC163.097

Design of Pore Silicon Carbide for Transferring Li^+, Na^+, K^+ in Biological Cells by DFT Study

Fatemeh Mollaamin [1,*], **Majid Monajjemi** [2]

[1] Department of Biomedical Engineering, Faculty of Engineering and Architecture, Kastamonu University, Kastamonu, Turkey
[2] Department of Biology, Faculty of Science, Kastamonu University, Kastamonu, Turkey
* Correspondence: fmollaamin@kastamonu.edu.tr;

Received: 23.08.2025; Accepted: 27.10.2025; Published: 15.06.2026

Abstract: Alkali Metal ions play vital roles in biology. Many of them are crucial for catalysis, electron transport, and the fixation, detection, or metabolism of gas molecules. Silicon carbide (SiC)-based nanomaterials have shown promising applications and higher performance in the biological arena. A vast study on ion transport by $SiLi^+C$, $SiNa^+C$, and SiK^+C complexes was probed using computational approaches due to density state analysis of charge density differences (CDD), total density of state (TDOS), and molecular electrostatic potential (ESP) for hybrid clusters of $SiLi^+C$, $SiNa^+C$, and SiK^+C. Functionalizing of Li^+, Na^+, K^+ cations can augment the negative atomic charge of C2, C3, C7–C12, C14, C15, C17, C18, C22–C27, C29, C30 as electron acceptors in $SiLi^+C$, $SiNa^+C$ and SiK^+C nanoclusters. A small portion of Li^+, Na^+, and K^+ entered the Si–C layer to replace the alkali and alkaline earth metals sites, which could improve the structural stability of the electrode material at high multiplicity, thereby improving the capacity retention rate. $SiLi^+C$, $SiNa^+C$, SiK^+C nanoclusters have shown the steepest maximums TDOS surrounding –0.30, –0.40, –0.50, and –0.60 a.u. owing to the covalent bond between Li^+, Na^+, K^+ cations and SiC nanostructure with a maximum density of state of ≈ 12. Higher Si/C content can increase ion transport capacity through $SiLi^+C$, $SiNa^+C$, and SiK^+C nanoclusters for the ion transport process and improve the rate performances by enhancing electrical conductivity. Finally, the unresolved issues, plausible challenges, current status, and future perspectives for the development and design of SiC have been summarized and are expected to promote the medical sectors.

Keywords: biological cell; ion transport; alkali metal ions; silicon carbide nanocluster; density of states.

© 2026 by the authors. This article is an open-access article distributed under the terms and conditions of the Creative Commons Attribution (CC BY) license (https://creativecommons.org/licenses/by/4.0/), which permits unrestricted use, distribution, and reproduction in any medium, provided the original work is properly cited. The authors retain copyright of their work, and no permission is required from the authors or the publisher to reuse or distribute this article, as long as proper attribution is given to the original source.

1. Introduction

The alkali metals and alkaline-earth metals always have similar electronic structures and chemical properties. Therefore, they usually coexist in ores or water resources. The separation of alkali metal ions and alkaline-earth metal ions has significant application prospects in seawater desalination, resource recovery, and energy storage, which are paramount for the sustainable development of the environment, resources, and energy. Membrane technologies have been extensively investigated in this area and have attracted widespread

attention due to their environmental friendliness and energy efficiency. Recently, progress in membrane technology has focused on the separation of alkali and alkaline earth metal ions, including organic, inorganic, and mixed-matrix membranes [1].

While prominently represented in the environment, lithium ions are not essential cofactors in biological systems [2,3]. In contrast, sodium, potassium, calcium, and magnesium are essential cofactors in multiple biological systems, while others, such as iron, zinc, and copper, play roles in specific systems [4–7]. Thus, lithium ions appear to have been isolated from being incorporated as an essential element during the evolution of increasingly complex biological systems [8–10].

Irrespective of those who discovered Li salt's effects on patients with bipolar disorder, its use in these conditions became the standard for decades and continues today. In the treatment of bipolar disorder patients with lithium salts, it has been noted that not all patients are responsive to therapeutic doses of this intervention [11–13].

The nanomaterials, however, are widely applied in photocatalysis, energy, sensing, water purification, biomedicine, and electronics, with further material engineering for other future applications [14,15]. In fact, these are semiconductors in which the pure state of the semiconductor material is deliberately diluted by adding some quantities of impurities. By doing so, their conductivity and properties are improved compared to those of intrinsic semiconductors.

As the effect of Li salt utilization as a replacement for NaCl was an obvious failure, its successful usage in the treatment of bipolar disorder in patients was a stimulus from several outlooks for a more detailed research of Li salt's impacts on other biological systems, with the emergence of a better understanding of its broad significance in biology and its functions as a modulator or regulator of biological systems. It performs a critical task in monitoring alterations in the system, entirely owing to genetic or biological heterogeneity in humans [16–22].

Currently, the present research aims to explore the possibility of using SiC nanocage for ion transport of Li^+, $Na^{+,}$ and K^+ by employing first-principles calculations. We have analyzed the structural and electronic properties of $SiLi^+C$, $SiNa^+C$, and SiK^+C nanoclusters using state-of-the-art computational techniques.

2. Materials and Methods

The aim of this study is to transport alkali metal ions of Li^+, Na^+, and K^+ by SiC nanocages towards the formation of $SiLi^+C$, $SiNa^+C$, and SiK^+C complexes (Figure 1a,b,c), which can increase the ion transfer in the cell membrane.

All calculations in this paper were performed with the first-principles method based on the density functional theory (DFT) method. The geometries optimization and vibrational frequencies analysis of the models were calculated using DFT with the hybrid exchange-correlation functional B3LYP and 6-311+G(d,p) basis sets. DFT has proven to be an essential tool for exploring the electronic and structural properties of graphene-based electrodes in lithium-ion batteries. While its effectiveness is evident in revealing atomic-level phenomena, current implementations face notable challenges, especially when dealing with complex systems involving defects, interfaces, and lithium diffusion. In this investigation, the computations have been launched by the Coulomb-attenuating method–(Becke, 3-parameter, Lee-Yang-Parr) [CAM–B3LYP–D3] level of theory. This highlights the importance of

considering the electronic correlation and dispersion effects in accurately predicting polarizabilities [23].

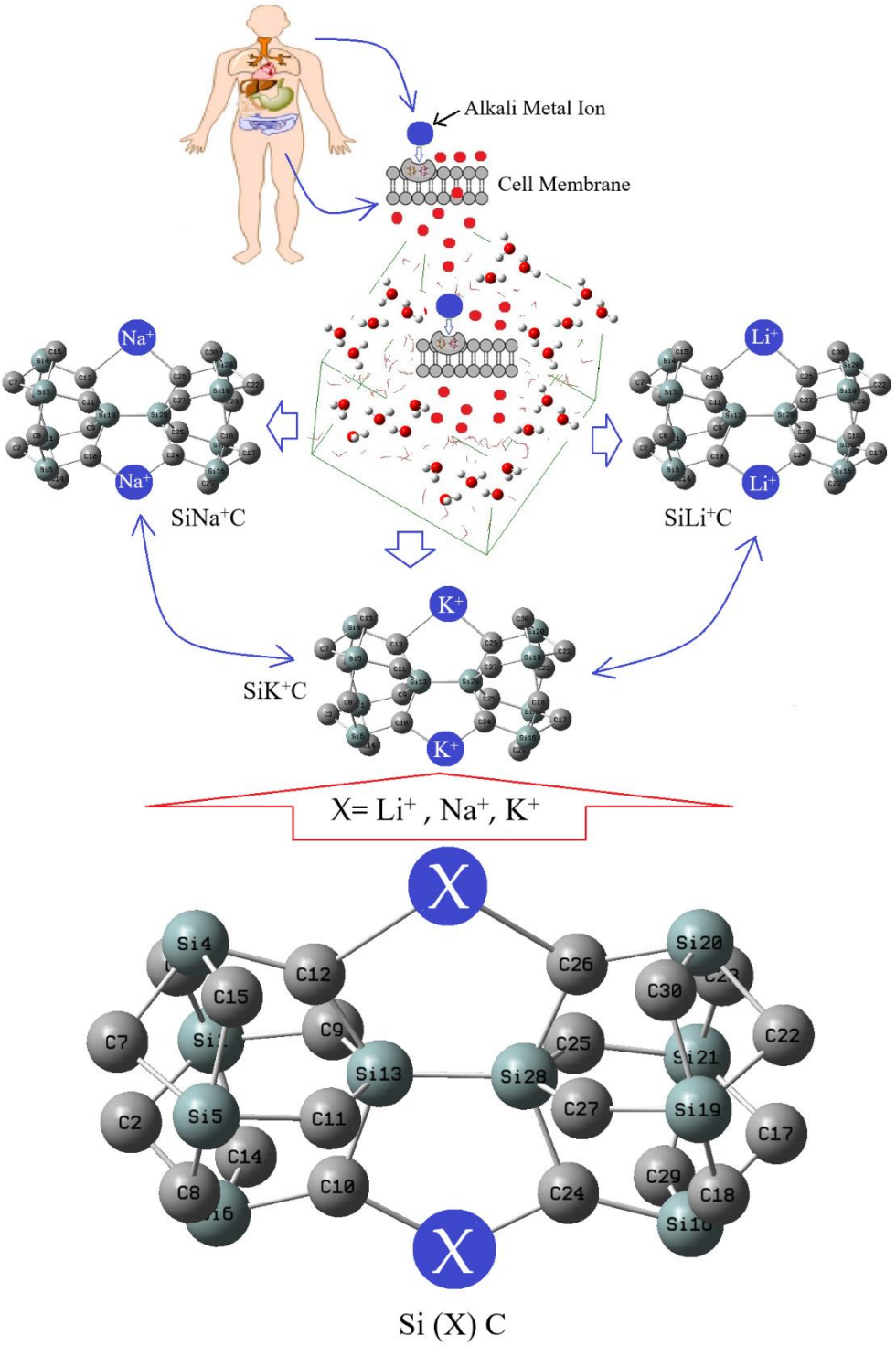

Figure 1. Adding Li^+, Na^+, and K^+ to SiC nanocluster and formation of **(a)** $SiLi^+C$; **(b)** $SiNa^+C$; **(c)** SiK^+C complexes towards ion transport in biological cells. Note: X in Figure is Li^+, Na^+, or K^+.

The analysis of the Bader charge parameter [24] has been illustrated for Ion transport by hybrid clusters of $SiLi^+C$, $SiNa^+C$, and SiK^+C complexes (Figure 1a,b,c) due to Gaussian 16 revision C.01 computational software [25] and GaussView 6.1 graphical program [26]. The applied basis sets for theoretical calculations of ion transport by $SiLi^+C$, $SiNa^+C$, and SiK^+C complexes have been supported by LANL2DZ and 6–311+G (d,p).

In this investigation, the Onsager model, developed by Frisch, Wong, and Wiberg, uses spherical cavities. Even though this implies a less accurate description of the solute-solvent interface, this approximation simplifies the evaluation of energy changes during geometry optimizations and frequency analyses. In fact, a cavity must have a physical sense, as in the Onsager model, and a mathematical ability, as is often the case in other descriptions of solvent effects [27]. On the other hand, the cavity must exclude the solvent and define its boundaries as the most probable region of the solute charge distribution [28].

The $Li^+/Na^+/K^+$ insertion might also result in the cleavage of some C–Li^+, C–Na^+, or C–K^+ bonds in the SiC nanocluster and the expansion, providing favorable sites for the subsequent ion insertion in the network (Figure 1a,b,c). At the same time, the Li^+, Na^+, or K^+ cations could react rapidly with silicon or carbide of SiC nanocluster to form $SiLi^+C$, $SiNa^+C$, and SiK^+C heteroclusters. The results obtained using the mentioned method shed light on the impact of the methodology choice on the predicted properties, emphasizing the need for careful consideration when analyzing and interpreting theoretical results across such diverse geometries.

3. Results and Discussion

3.1. Charge density differences analysis.

In Figure 2(a,b,c), charge density differences (CDD) [29] have been shown for $SiLi^+C$, $SiNa^+C$, and SiK^+C nanoclusters with the vibration in the district about –12 to +9 Bohr through co-interaction between alkali metal ions of Li+31–Li+32, Na+31–Na+32, and K+31–K+32.

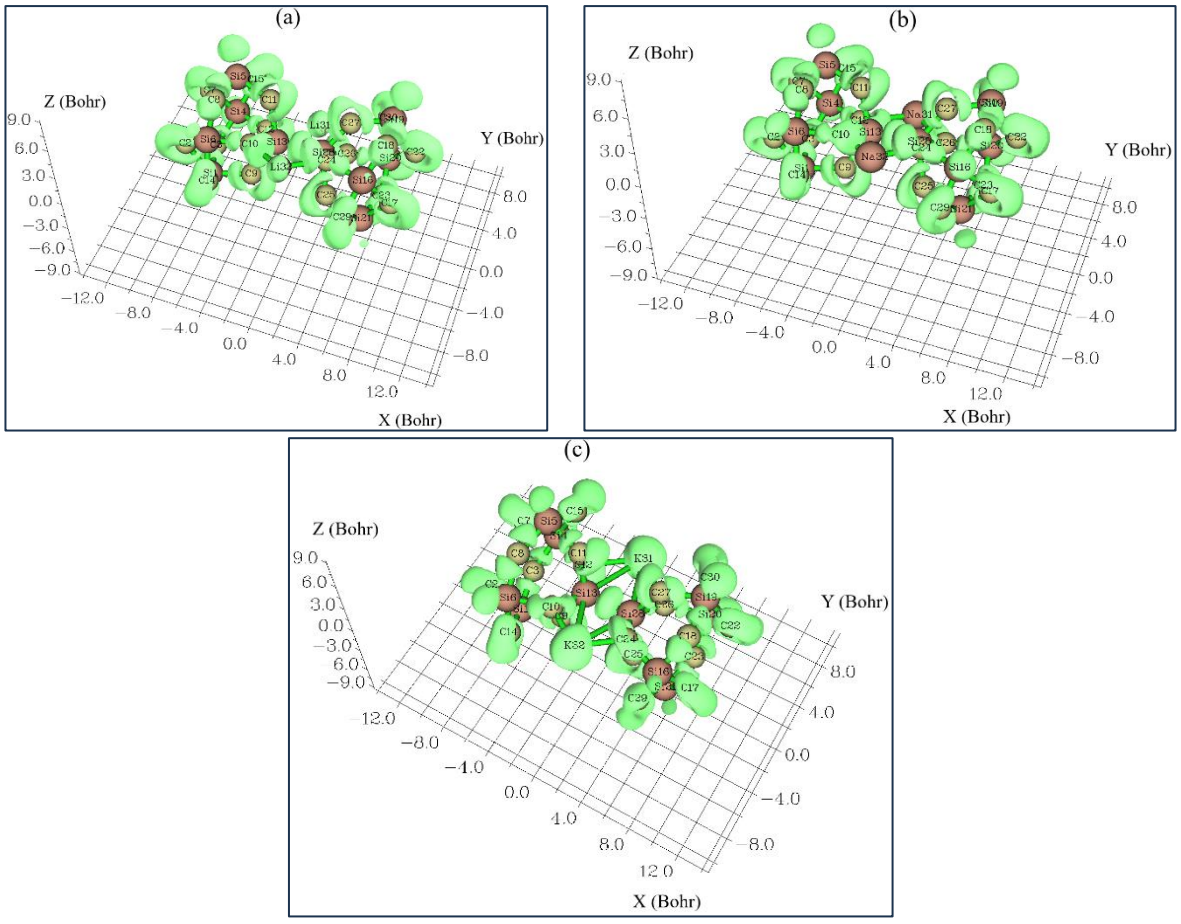

Figure 2. CDD graphs for **(a)** $SiLi^+C$; **(b)** $SiNa^+C$; **(c)** SiK^+C nanoclusters.

Moreover, the elements of C2, C3, C7–C12, C14, C15, C17, C18, C22–C27, C29, C30 from $SiLi^+C$, $SiNa^+C$, and SiK^+C nanoclusters have displayed the vibration about –12 to +9 Bohr (Figure 2a,b,c).

The charge distribution has been illustrated during alkali metal ions captured by SiC nanostructure towards the formation of $SiLi^+C$, $SiNa^+C$, and SiK^+C nanoclusters, respectively (Table 1).

Table 1. The atomic charge (Q/coulomb) for $SiLi^+C$, $SiNa^+C$ and SiK^+C nanoclusters.

$SiLi^+C$		**$SiNa^+C$**		**SiK^+C**	
Atom/Ion	Q	Atom/Ion	Q	Atom/Ion	Q
Li^+31	0.75	Na^+31	0.68	K^+31	0.91
Li^+32	0.50	Na^+32	0.37	K^+32	0.90
C2	–0.42	C2	–0.42	C2	–0.43
C3	–0.34	C3	–0.37	C3	–0.34
C7	–0.38	C7	–0.40	C7	–0.39
C8	–0.36	C8	–0.37	C8	–0.37
C9	–0.38	C9	–0.37	C9	–0.37
C10	–0.81	C10	–0.70	C10	–1.01
C11	–0.37	C11	–0.35	C11	–0.32
C12	–0.92	C12	–0.82	C12	–0.90
C14	–0.37	C14	–0.37	C14	–0.36
C15	–0.38	C15	–0.38	C15	–0.41
C17	–0.41	C17	–0.42	C17	–0.43
C18	–0.35	C18	–0.37	C18	–0.38
C22	–0.38	C22	–0.40	C22	–0.40
C23	–0.34	C23	–0.38	C23	–0.36
C24	–0.78	C24	–0.69	C24	–0.96
C25	–0.34	C25	–0.34	C25	–0.32
C26	–0.85	C26	–0.75	C26	–0.91
C27	–0.51	C27	–0.47	C27	–0.46
C29	–0.40	C29	–0.39	C29	–0.42
C30	–0.37	C30	–0.39	C30	–0.37

Functionalizing of Li^+, Na^+, K^+ cations can augment the negative atomic charge of C2, C3, C7–C12, C14, C15, C17, C18, C22–C27, C29, C30 as electron acceptors in $SiLi^+C$, $SiNa^+C$ and SiK^+C nanoclusters (Figure 3a,b,c).

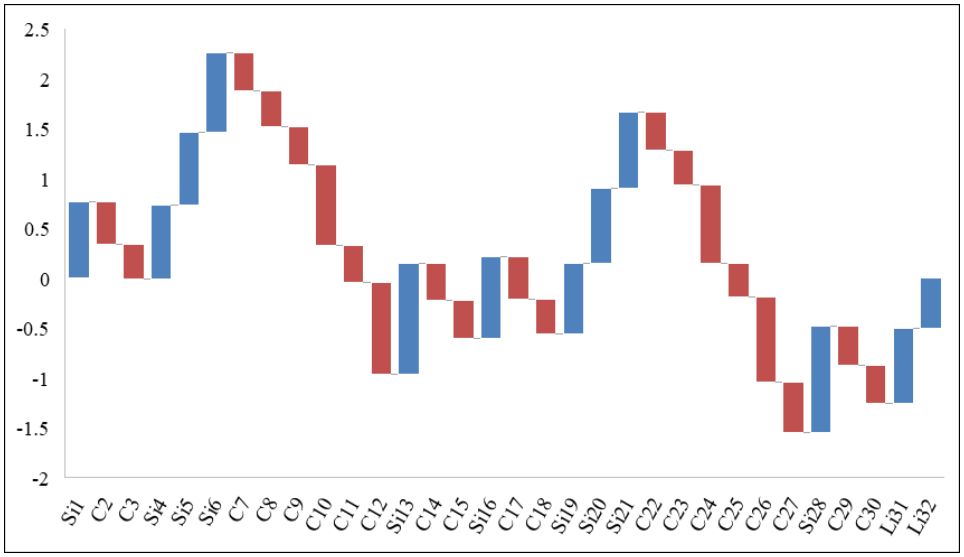

(a)

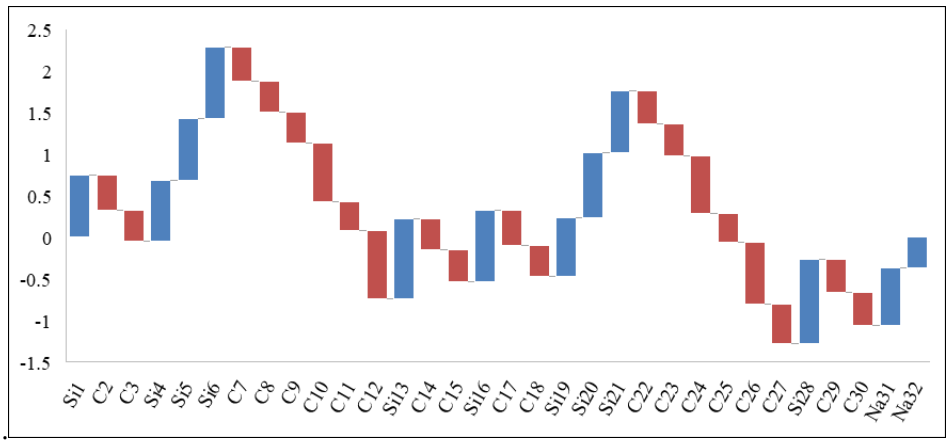

(b)

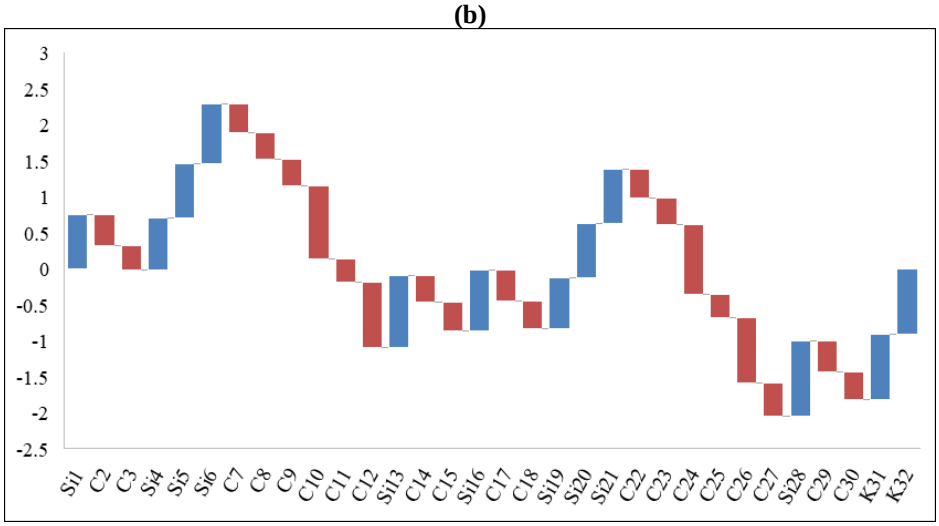

(c)

Figure 3. The changes of charge distribution for **(a)** $SiLi^+C$; **(b)** $SiNa^+C$; **(c)** SiK^+C nanoclusters.

3.2. Total density of states.

In an isolated system (such as a molecule), the energy levels are discrete; the concept of "density of state (DOS)" is supposed to be completely valueless in this situation. Therefore, the "original total DOS (TDOS)" of an isolated system can be written as using the "Multiwfn" [30, 31] program.

In the "TDOS map", each discrete vertical line corresponds to a "molecular orbital (MO)", and the dashed line highlights the position of "HOMO". The curve is the "TDOS" simulated based on the distribution of "MO" energy levels.

Regarding ion transport by $SiLi^+C$, $SiNa^+C$, and SiK^+C nanoclusters, TDOS has been evaluated. This factor can demonstrate the existence of important chemical interactions often on the "convex side" (Figure 4 a,b,c).

$SiLi^+C$, $SiNa^+C$, SiK^+C nanoclusters (Figure 4a,b,c) have shown the steepest maximums TDOS surrounding –0.30,–0.40, –0.50, and –0.60 a.u. owing to the covalent bond between Li^+, Na^+, K^+ cations and SiC nanostructure with a maximum density of state of ≈ 12.

Fragment 1 has been defined for C9 to C12, Si13, C24 to C27, Si28, and X31/X32 ($X=Li^+$, Na^+, K^+) in Figure 4 (a,b,c). Fragment 2 has indicated the fluctuation of Si1, Si4, to Si6 beside the similar involved atoms of Fragment 1 in Figure 4 (a,b,c). Finally, it was considered the fluctuation of Si16, Si19 to Si21, C17, C18, C22, C23, C29, C30 in Figure 4 (a,b,c).

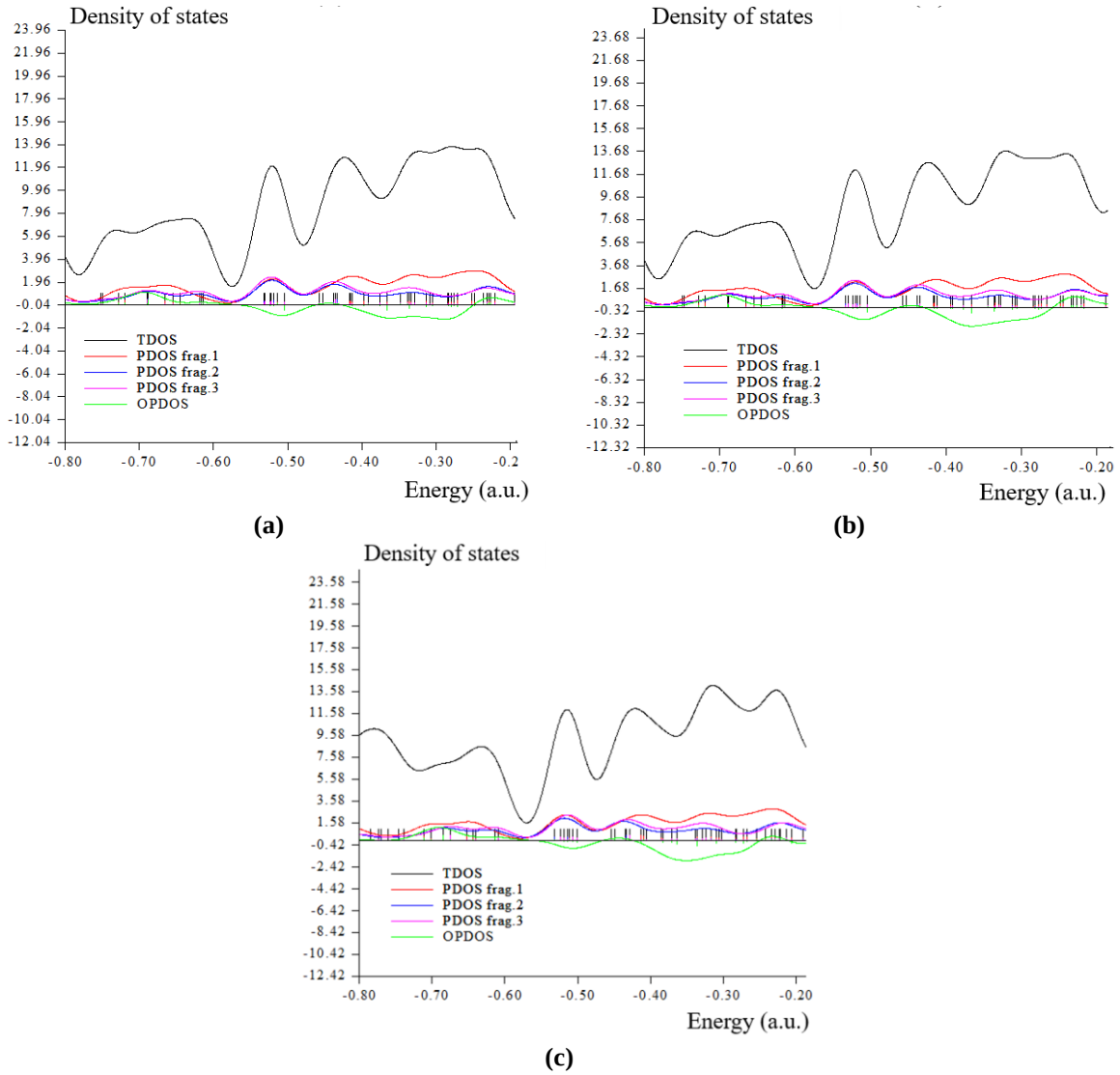

Figure 4. OPDOS/PDOS/TDOS graphs of **(a)** $SiLi^+C$; **(b)** $SiNa^+C$; **(c)** SiK^+C nanoclusters.

3.3. Molecular electrostatic potential (ESP).

Trapping of Li^+, Na^+, and K^+ cations by SiC nanostructure (Figure 5a,b,c) towards the formation of $SiLi^+C$, $SiNa^+C$, and SiK^+C nanoclusters might be described by molecular electrostatic potential (ESP) [32] graphs using Multiwfn [30, 31] due to achieving their delocalization/localization characterizations of electrons and chemical bonds (Figure 5a,b,c).

$SiLi^+C$ (Figure 5a), $SiNa^+C$ (Figure 5b), SiK^+C (Figure 5c) have demonstrated the electron delocalization through an isosurface map with labeling atoms of C10, C12, Si13, C24, C26, Si28, X31/X32 (X=Li^+, Na^+, K^+). In fact, the counter map of ESP can confirm that $SiLi^+C$, $SiNa^+C$, and SiK^+C nanoclusters may augment the efficiency of ion transport (Figure 5a,b,c).

Besides, the intermolecular orbital overlap integral is important in the illustration of intermolecular charge transfer, which can compute HOMO-HOMO and LUMO-LUMO overlap integrals between Li^+, Na^+, K^+ cations and SiC nanostructure. The layered silicon carbide improved by alkali metal ions of lithium (1+), sodium (1+), and potassium (1+) has indicated the structural stability of Li^+-, Na^+-, and K^+-ion heteroclusters through the reported stability energies in Table 2. Moreover, the intermolecular orbital overlap integral is important in discussions of intermolecular charge transfer, which can calculate HOMO-HOMO and LUMO-LUMO overlap integrals between the alkali metal ions and silicon carbide. The wavefunction level we used was CAM–B3LYP–D3/6–311+G(d,p) that corresponds to HOMO

and LUMO, respectively (Table 2). Therefore, E_{LUMO} (a.u.), E_{LUMO} (a.u.), and the local bandgap energies (ΔE/a.u.) and immobile charges induced by polarization discontinuity are simultaneously controlled throughout the structures, and optimized band profiles are eventually achieved for $SiLi^+C$, $SiNa^+C$, and SiK^+C nanoclusters (Table 2).

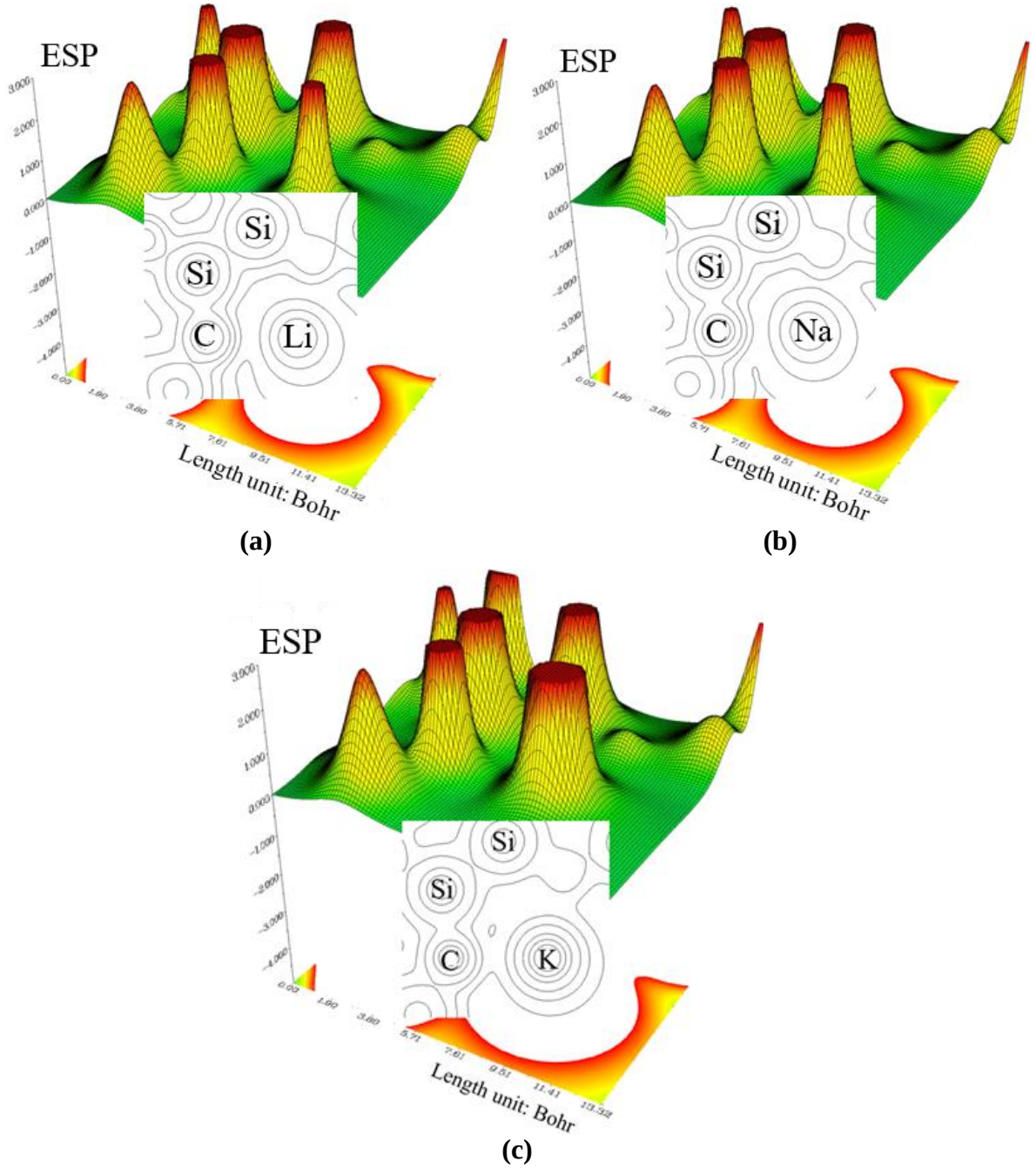

Figure 5. The counter (right side) and shaded (left side) maps of ESP graphs for **(a)** $SiLi^+C$; **(b)** $SiNa^+C$; **(c)** SiK^+C nanoclusters.

Table 2. Stability energy (kcal/mol), dipole moment (debye), LUMO (eV), HOMO (eV), energy gap (ΔE) (eV), and cell capacity (C, mAh g^{-1}) for $SiLi^+C$, $SiNa^+C$, and SiK^+C nanoclusters.

Heteroclusters	$E_s \times 10^{-3}$ (kcal/mol)	Dipole moment (debye)	E_{HOMO} (eV)	E_{LUMO} (eV)	$\Delta E = E_{LUMO} - E_{HOMO}$ (eV)	C (C, mAhg^{-1})
$SiLi^+C$	-509.21	1.25	-5.20	-4.20	1.00	100.20
$SiNa^+C$	-499.96	1.18	-4.96	-4.43	0.52	94.53
SiK^+C	-534.83	0.94	-5.05	-4.13	0.92	453.14

A small portion of Li^+, Na^+, and K^+ entered the Si–C layer to replace the alkali metal ions sites, which could improve the structural stability of the nanocluster at high multiplicity,

thereby improving the capacity retention rate of 100.2018, 94.5295, 198.8630, and 188.1862 $mAhg^{-1}$ for $SiLi^+C$, $SiNa^+C$, and SiK^+C complexes, respectively (Table 2) [33].

In addition, the amount of "Mayer bond order" [34] is generally according to empirical bond order, for the single bond is near 1.0. "Mulliken bond order" [35], with a small accord with empirical bond order, is not appropriate for quantifying bonding strength, for which Mayer bond order always performs better. However, "Mulliken bond order" is a good qualitative indicator for "positive amount" of bonding and "negative amount" of antibonding, which are evacuated and localized, respectively (Table 3).

Table 3. The bond order of Mayer, Wiberg, Mulliken, Laplacian, and Fuzzy from mixed alpha and beta density matrix for $SiLi^+C$, $SiNa^+C$, and SiK^+C nanoclusters.

Compound	Bond type	Bond order				
		Mayer	Wiberg	Mulliken	Laplacian	Fuzzy
$SiLi^+C$	Si13–Si28	0.73	0.67	0.56	0.41	0.90
	C10–Li^+32	0.40	0.42	0.48	0.43	0.36
	C12–Li^+31	0.16	0.26	0.27	0.2	0.18
	C24–Li^+32	0.36	0.41	0.44	0.42	0.34
	C26–Li^+31	0.20	0.31	0.31	0.40	0.22
$SiNa^+C$	Si13–Si28	0.69	0.66	0.42	0.47	0.87
	C10–Na^+32	0.41	0.27	0.59	0.60	0.53
	C12–Na^+31	0.16	0.20	0.32	0.31	0.33
	C24–Na^+32	0.41	0.27	0.56	0.53	0.51
	C26–Na^+31	0.22	0.23	0.37	0.36	0.40
SiK^+C	Si13–Si28	0.76	0.66	0.97	0.93	0.86
	C10–K^+32	0.57	0.39	0.54	0.53	0.60
	C12–K^+31	0.24	0.23	0.11	0.10	0.35
	C24–K^+32	0.58	0.38	0.42	0.40	0.58
	C26–K^+31	0.36	0.29	0.20	0.19	0.42

As shown in Table 3, “Laplacian bond order” [36] shows a strong correlation with bond polarity, bond dissociation energy, and bond vibrational frequency. The low value of the Laplacian bond order might indicate that it is insensitive to the level of calculation used to produce the electron density. Generally, the value of “Fuzzy bond order” is close to the Mayer bond order, especially for low-polar bonds, but is much more stable with respect to changes in basis set. Computation of “Fuzzy bond order” demands running “Becke's DFT” numerical integration, owing to which the calculation value is larger than the assessment of “Mayer bond order”, and it can be more precise [37].

4. Conclusions

Li^+, Na^+, and K^+ metal ions captured by silicon carbide towards the formation of $SiLi^+C$, $SiNa^+C$, and SiK^+C nanoclusters were studied by computational methods. The changes in charge density defined a notable charge transfer in $SiLi^+C$, $SiNa^+C$, and SiK^+C. Due to the semiconducting nature of SiC, it is usually composited with C for better ionic and electronic conductivities. It is well established that enhancing Li^+, Na^+, or K^+ in biological cells can augment the ion transport. Functionalizing of Li^+, Na^+, K^+ cations can augment the negative atomic charge of C2, C3, C7–C12, C14, C15, C17, C18, C22–C27, C29, C30 as electron acceptors in $SiLi^+C$, $SiNa^+C$ and SiK^+C nanoclusters. The results of this research article indicate that the architectural design of $X_2(SiC)$ ($X = Li^+$, Na^+, K^+) can augment the capacity of biological cells. $SiLi^+C$, $SiNa^+C$, SiK^+C nanoclusters have shown the steepest maximums TDOS surrounding –0.30, –0.40, –0.50, and –0.60 a.u. owing to the covalent bond between

Li^+, Na^+, K^+ cations and SiC nanostructure with a maximum density of state of ≈ 12. A small portion of Li^+, Na^+, or K^+ entered the Si–C layer to replace the alkali metal ions sites, which could improve the structural stability of the electrode material at high multiplicity, thereby improving the capacity retention rate of 100.2018, 94.5295, 198.8630, and 188.1862 $mAhg^{-1}$ for $SiLi^+C$, $SiNa^+C$, and SiK^+C complexes, respectively. We presented that the ionic groups on the side chain of the nanocluster with smaller steric space should provide higher ionic conductivity due to their lower rotation energy barriers. This research article covers the state-of-the-art synthetic strategies used to prepare the materials, the basic structure, and a panorama of different optimization strategies that lead to improved physicochemical properties responsible for biological applications.

Author Contributions

Conceptualization, F.M.; methodology, F.M.; software, F.M.; validation, F.M. and M.M.; formal analysis, F.M. and M.M.; investigation, F.M. and M.M.; resources, F.M. and M.M.; data curation, F.M.; writing—original draft preparation, F.M.; writing—review and editing, M.M.; visualization, F.M. and M.M.; supervision, F.M.; project administration. The author has read and agreed to the published version of the manuscript.

Institutional Review Board Statement

Not applicable.

Informed Consent Statement

Not applicable.

Data Availability Statement

Not applicable.

Funding

This research received no external funding.

Acknowledgments

The authors are grateful to Kastamonu University for successfully completing this paper and its research.

Conflict of Interest

The author declares no conflict of interest.

References

1. Hart, D.A. Lithium Ions as Modulators of Complex Biological Processes: The Conundrum of Multiple Targets, Responsiveness and Non-Responsiveness, and the Potential to Prevent or Correct Dysregulation of Systems during Aging and in Disease. *Biomolecules* **2024**, *14*, 905, https://doi.org/10.3390/biom14080905.
2. Herrera-Rivero, M.; Gutierrez-Fragosa, K.; International consortium on lithium genetics (ConLi + Gen); Kurtz, J.; Baune, B.T. Immunogenetics of lithium response and psychiatric phenotypes in patients with bipolar disorder. *Transl. Psychiatry* **2024**, *14*, 174, https://doi.org/10.1038/s41398-024-02865-4.

3. Kraytsberg, A.; Eli, Y.E. Biomaterials for advanced Li and Li-ion batteries. *J Solid State Electrochem* **2025**. https://doi.org/10.1007/s10008-025-06268-3.
4. Razzaque, M.S.; Wimalawansa, S.J. Minerals and Human Health: From Deficiency to Toxicity. *Nutrients* **2025**, *17*, 454, https://doi.org/10.3390/nu17030454.
5. Tian, L.; Andrews, C.; Yan, Q.; Yang, J.J. Molecular regulation of calcium-sensing receptor (CaSR)-mediated signaling. *Chronic Dis. Transl. Med.* **2024**, *10*, 167–194, https://doi.org/10.1002/cdt3.123.
6. Singulani, M.P.; Fernandes-Ferreira, A.F.; Figueroa, P.S.; Cuyul-Vasquez, I.; Talib, L.L.; Britto, L.R.; Forlenza, O.V. Lithium and disease modification: A systematic review and meta-analysis in Alzheimer's and Parkinson's disease. *Ageing Res. Rev.* **2024**, *95*, 102231, https://doi.org/10.1016/j.arr.2024.102231.
7. Dean, B.; Scarr, E. Common changes in rat cortical gene expression after valproate or lithium treatment paricularly affect pre- and post-synaptic pathways that regulate four neurotransmitters systems. *World J. Biol. Psychiatry* **2024**, *25*, 54–64, https://doi.org/10.1080/15622975.2023.2258972.
8. Phelps, J.; Coskey, O.P. Low and very low lithium levels: Thyroid effects are small but still require monitoring. *Bipolar Disord.* **2024**, *26*, 129–135, https://doi.org/10.1111/bdi.13377.
9. Gelman, K.; Melott, J.; Thakur, V.; Tarabishy, A.R.; Brandt, A.; Konrad, P.; Ranjan, M.; Memon, A.A. MR-guided focused ultrasound thalamotomy for lithium-induced tremor: A case report and literature review. *Front. Neurol.* **2024**, *14*, 1331241, https://doi.org/10.3389/fneur.2023.1331241.
10. Herrera-Rivero, M.; Gutierrez-Fragosa, K. International consortium on lithium genetics (ConLi + Gen); Kurtz, J.; Baune, B.T. Immunogenetics of lithium response and psychiatric phenotypes in patients with bipolar disorder. *Transl. Psychiatry* **2024**, *14*, 174, https://doi.org/10.1038/s41398-024-02865-4.
11. Bucatoș, B.-O.; Gaita, L.; Romoșan, A.-M.; Papava, I.; Popovici, M.; Romoșan, R.-Ș.; Bondrescu, M.; Daescu, A.-M.C.; Dehelean, L. Coping Strategies in Patients with Bipolar Disorder (BD) and Major Depressive Disorder (MDD) and Their Correlation with Clusters of Psychiatric Symptoms. *Healthcare* **2025**, *13*, 1050, https://doi.org/10.3390/healthcare13091050.
12. Zafar, M.S.; Salimi, P.; Ricci, M.; Zia, J.; Zaccaria, R.P. Environmentally Sustainable Anode Material for Lithium-Ion Batteries Derived from Cattle Bone Waste: A Full-Cell Analysis with a $LiFePO_4$ Cathode. *Sustainability*. **2025**, *17*, 3005, https://doi.org/10.3390/su17073005.
13. Ramushu, P.; Mangoakoane, D.D.; Makola, R.T.; Matsebatlela, T.M. Lithium Induces Oxidative Stress, Apoptotic Cell Death, and G2/M Phase Cell Cycle Arrest in A549 Lung Cancer Cells. *Molecules* **2025**, *30*, 1797, https://doi.org/10.3390/molecules30081797.
14. Ju, S.; Singh, M.K.; Han, S.; Ranbhise, J.; Ha, J.; Choe, W.; Yoon, K.-S.; Yeo, S.G.; Kim, S.S.; Kang, I. Oxidative Stress and Cancer Therapy: Controlling Cancer Cells Using Reactive Oxygen Species. *Int. J. Mol. Sci.* **2024**, *25*, 12387, https://doi.org/10.3390/ijms252212387.
15. Zafrilla-Lopez, M.; Acosta-Diez, M.; Mitjans, M.; Gimenez-Palomo, A.; Saiz, P.A.; Barrot-Feixat, C.; Jimenez, E.; Papiol, S.; Ruiz, V.; Gavin, P. Lithium response in bipolar disorder: Epigenome-wide DNA methylation signatures and epigenetic aging. *Eur. Neuropsychopharmacol.* **2024**, *85*, 23-31, https://doi.org/10.1016/j.euroneuro.2024.03.010.
16. Ghani, F.; An, K.; Lee, D. A Review on Design Parameters for the Full-Cell Lithium-Ion Batteries. *Batteries* **2024**, *10*, 340, https://doi.org/10.3390/batteries10100340.
17. Mollaamin, F. Anchoring of 2D layered materials of $Ge_5Si_5O_{20}$ for (Li/Na/K)-(Rb/Cs) batteries towards Eco-friendly energy storage. *BMC Chem.* **2025**, *19*, 233, https://doi.org/10.1186/s13065-025-01593-0.
18. Rijal, S.; Jang, S.H.; Park, S.J.; Han, S.K. Lithium Enhances the GABAergic Synaptic Activities on the Hypothalamic Preoptic Area (hPOA) Neurons. *Int. J. Mol. Sci.* **2021**, *22*, 3908, https://doi.org/10.3390/ijms22083908.
19. Marchese, D.; Giosuè, C.; Staffolani, A.; Conti, M.; Orcioni, S.; Soavi, F.; Cavalletti, M.; Stipa, P. An Overview of the Sustainable Recycling Processes Used for Lithium-Ion Batteries. *Batteries* **2024**, *10*, 27, https://doi.org/10.3390/batteries10010027.
20. Asamoah, G.A.; Korsah, M.; Jeyasundar, P.G.S.A.; Ahmed, M.; Lau, S.Y.; Danquah, M.K. Nanotechnology-Based Lithium-Ion Battery Energy Storage Systems. *Sustainability* **2024**, *16*, 9231, https://doi.org/10.3390/su16219231.
21. Mollaamin, F. Competitive Intracellular Hydrogen-Nanocarrier Among Aluminum, Carbon, or Silicon Implantation: a Novel Technology of Eco-Friendly Energy Storage using Research Density Functional Theory. *Russ. J. Phys. Chem. B* **2024**, *18*, 805–820, https://doi.org/10.1134/S1990793124700131.
22. Mollaamin, F.; Monajjemi, M. Nanomaterials for Sustainable Energy in Hydrogen-Fuel Cell: Functionalization and Characterization of Carbon Nano-Semiconductors with Silicon, Germanium, Tin or

Lead through Density Functional Theory Study. *Russ. J. Phys. Chem. B* **2024**, *18*, 607–623, https://doi.org/10.1134/S1990793124020271.
23. Benalia, A.; Boukaoud, A.; Amrani, R.; Krid, A. A B3LYP-D3 computational study of electronic, structural and torsional dynamic properties of mono-substituted naphthalenes: the effect of the nature and position of substituent. *J Mol Model* **2024**, *30*, 88, https://doi.org/10.1007/s00894-024-05884-6.
24. Zhou, X.; Cheng, Y.; Xu, X.; Zhang, L.; Tian, S.; Xu, X.; Guo, B.; Tang, W.; Yan, C.; Qian, T. Bader Charge Balance Mechanism Realizes Industrial-Grade Current Hydrogen Production. *Inorg. Chem.* **2025**, *64*, 14118–14127, https://doi.org/10.1021/acs.inorgchem.5c00590.
25. Frisch, M.J.; Trucks, G.W.; Schlegel, H.B.; Scuseria, G.E.; Robb, M.A.; Cheeseman, J.R.; Scalmani, G.; Barone, V.; Petersson, G.A.; Nakatsuji, H.; Li, X.; Caricato, M.; Marenich, A.V.; Bloino, J.; Janesko, B.G.; Gomperts, R.; Mennucci, B.; Hratchian, H.P.; Ortiz, J. V.; Izmaylov, A. F.; Sonnenberg, J.L.; Williams-Young, D.; Ding, F.; Lipparini, F.; Egidi, F.; Goings, J.; Peng, B.; Petrone, A.; Henderson, T.; Ranasinghe, D.; Zakrzewski, V.G.; Gao, J.; Rega, N.; Zheng, G.; Liang, W.; Hada, M.; Ehara, M.; Toyota, K.; Fukuda, R.; Hasegawa, J.; Ishida, M.; Nakajima, T.; Honda, Y.; Kitao, O.; Nakai, H.; Vreven, T.; Throssell, K.; Montgomery, J.A., Jr.; Peralta, J.E.; Ogliaro, F.; Bearpark, M.J.; Heyd, J.J.; Brothers, E.N.; Kudin, K.N.; Staroverov, V.N.; Keith, T.A.; Kobayashi, R.; Normand, J.; Raghavachari, K.; Rendell, A.P.; Burant, J.C.; Iyengar, S.S.; Tomasi, J.; Cossi, M.; Millam, J.M.; Klene, M.; Adamo, C.; Cammi, R.; Ochterski, J.W.; Martin, R.L.; Morokuma, K.; Farkas, O.; Foresman, J.B.; Fox, D.J. Gaussian 16, Revision C.01, Gaussian, Inc., Wallingford CT, **2016**.
26. Dennington, R.; Keith Todd, A.; Millam John, M. GaussView, Version 6.06.16. Semichem Inc., Shawnee Mission, KS, USA, **2016**.
27. Chen, H.; Liu, H.; Xu, X. The Onsager principle and structure preserving numerical schemes. *Journal of Computational Physics* **2025**, *523*, 113679, https://doi.org/10.1016/j.jcp.2024.113679.
28. Wada, T.; Scarfone, A.M. Onsager's Non-Equilibrium Thermodynamics as Gradient Flow in Information Geometry. *Entropy* **2025**, *27*, 710, https://doi.org/10.3390/e27070710.
29. Xu, Z.; Qin, C.; Yu, Y.; Jiang, G.; Zhao, L. First-principles study of adsorption, dissociation, and diffusion of hydrogen on α-U (110) surface. *AIP Advances* **2024**, *14*, 055114, https://doi.org/10.1063/5.0208082.
30. Lu, T.; Chen, F. Multiwfn: A multifunctional wavefunction analyzer. *J. Comput. Chem.* **2012**, *33*, 580–592, https://doi.org/10.1002/jcc.22885.
31. Lu, T. A comprehensive electron wavefunction analysis toolbox for chemists, Multiwfn. *J. Chem. Phys.* **2024**, *161*, 082503, https://doi.org/10.1063/5.0216272.
32. Murray, J.S.; Riley, K.E.; Brinck, T. A Revival of Molecular Surface Electrostatic Potential Statistical Quantities: Ionic Solids and Liquids. *Crystals* **2024**, *14*, 995, https://doi.org/10.3390/cryst14110995.
33. Abrosimov, R.; Moosmann, B. The HOMO-LUMO Gap as Discriminator of Biotic from Abiotic Chemistries. *Life* **2024**, *14*, 1330, https://doi.org/10.3390/life14101330.
34. Mayer, I. Improved definition of bond orders for correlated wave functions. *Chem. Phys. Lett.* **2012**, *544*, 83–86, https://doi.org/10.1016/j.cplett.2012.07.003.
35. Ganguly, A.; Murthy, V.; Kannoorpatti, K. Structural and electronic properties of chromium carbides and Fe-substituted chromium carbides. *Mater. Res. Express* **2020**, *7*, 056508, https://doi.org/10.1088/2053-1591/ab8cf9.
36. Lu, T.; Chen, F. Bond Order Analysis Based on the Laplacian of Electron Density in Fuzzy Overlap Space. *J. Phys. Chem. A* **2013**, *117*, 3100–3108, https://doi.org/10.1021/jp4010345.
37. Wang, X.; Zhang, X.; Pedrycz, W.; Yang, S-H.; Boutat, D. Consensus of T-S Fuzzy Fractional-Order, Singular Perturbation, Multi-Agent Systems. *Fractal Fract.* **2024**, *8*, 523, https://doi.org/10.3390/fractalfract8090523.

Publisher's Note & Disclaimer

The statements, opinions, and data presented in this publication are solely those of the individual author(s) and contributor(s) and do not necessarily reflect the views of the publisher and/or the editor(s). The publisher and/or the editor(s) disclaim any responsibility for the accuracy, completeness, or reliability of the content. Neither the publisher nor the editor(s) assume any legal liability for any errors, omissions, or consequences arising from the use of the information presented in this publication. Furthermore, the publisher and/or the editor(s) disclaim any liability for any injury, damage, or loss to persons or property that may result from the use of any ideas, methods, instructions, or products mentioned in the content. Readers are encouraged to independently verify any

information before relying on it, and the publisher assumes no responsibility for any consequences arising from the use of materials contained in this publication.